ChemPubSoc Europe

DOI: 10.1002/chem.201402077

CHEMISTRY A European Journal Full Paper

Supramolecular Chemistry

H-Aggregates of Oligophenyleneethynylene (OPE)-BODIPY Systems in Water: Guest Size-Dependent Encapsulation Mechanism and Co-aggregate Morphology**

Naveen Kumar Allampally, Alexander Florian, María José Mayoral, Christina Rest, Vladimir Stepanenko, and Gustavo Fernández*[a]

Dedicated to Professor Frank Würthner on the occasion of his 50th birthday.

Abstract: The synthesis of a new oligophenyleneethynylene (OPE)-4,4-difluoro-4-bora-3a,4a-diaza-*s*-indacene (BODIPY) bolaamphiphile **1** and its aqueous self-assembly are reported. Compound **1** forms H-type aggregates in aqueous and polar media, as demonstrated by UV/Vis and fluorescence experiments. Concentration-dependent ^{1}H NMR studies in CD_3CN reveal that the BODIPY units are arranged on top of each other into π-stacks with H-type excitonic coupling, as supported by ROESY NMR and theoretical calculations and visualized by Cryo-SEM studies. A detailed analysis of the spectral changes observed in temperature-dependent UV/Vis studies reveals that **1** self-assembles in a non-cooperative (isodesmic) fashion in water. The hydrophobic interior of these self-assembled structures can be exploited to encapsulate hydrophobic dyes, such as tetracene and anthracene. Both dyes absorb in a complementary region of the UV/Vis spectrum and are small enough to interact with the hydrophobic segments of **1**. Temperature-dependent UV/Vis studies reveal that the spectral changes associated to the encapsulation mechanism of tetracene can be fitted to a Boltzmann function, and the initially flexible fibres of **1** rigidify upon guest addition. In contrast, the co-assembly of **1** and anthracene is a highly cooperative process, which suggests that a different class of (more-ordered) aggregates is formed. TEM and Cryo SEM imaging show the formation of uniform spherical nanoparticles, indicating that a subtle change in the guest molecular structure induces a significant change in the encapsulation mechanism and, consequently, the aggregate morphology.

Introduction

The exceptional optical and electronic properties of 4,4-difluoro-4-bora-3a,4a-diaza-*s*-indacene (BODIPY) dyes[1] have facilitated their implementation as fluorescent indicators,[2] laser dyes,[3] biolabeling[4] and photodynamic therapy agents[5] or active materials for optoelectronics[6] in recent years. For most of these applications, the investigation of the self-assembly pathways and bulk-state organization of the dye molecules is a prerequisite.[7] BODIPY derivatives are known to self-assemble through stacking of their dipyrromethene core,[8] which has been exploited to construct dye aggregates primarily in organic solvents[9] and in the bulk or liquid crystal state.[10] In contrast, extended aggregates of amphiphilic BODIPY dyes in water[11] remain unexplored, despite the great relevance of amphiphilic π-systems[12] in a large number of natural supramolecular assemblies.[13] In particular, the understanding of the thermodynamic aspects and mechanisms by which these nano-objects self-assemble in aqueous medium or encapsulate and release guest molecules is of high relevance to the field of biomedicine.

To date, different forms of soft matter, in particular supramolecular gels,[14] have been used for the encapsulation of guest molecules for sensing applications, drug delivery, catalysis, or crystal growth. Encapsulation of guests by these assemblies can also produce new nanostructured architectures with innovative properties.[15] A particularly exciting approach is the utilization of nanofiber solutions and hydrogels as artificial 3D cell culture supports that mimic the natural extracellular medium,[16] which can even maintain mammalian cells in 3D environments for tissue regeneration applications.[17] The interface of artificial self-assembled structures with biological systems would certainly benefit from a better comprehension of the mechanisms taking place during binding, which might be exploited to control the morphology of the resulting co-aggregate structures.

In our group, we have recently reported the synthesis and self-assembly of a nonpolar oligophenyleneethynylene (OPE)-BODIPY derivative substituted with peripheral dodecyl chains

[a] *Dr. N. K. Allampally, A. Florian, Dr. M. J. Mayoral, C. Rest, Dr. V. Stepanenko, Dr. G. Fernández*
Institut für Organische Chemie and Center for Nanosystems Chemistry
Universität Würzburg Am Hubland, 97074 Würzburg (Germany)
Fax: (+49) 931-31-84756
E-mail: gustavo.fernandez@uni-wuerzburg.de

[**] *BODIPY = 4,4-difluoro-4-bora-3a,4a-diaza-s-indacene.*

Supporting information for this article is available on the WWW under http://dx.doi.org/10.1002/chem.201402077.

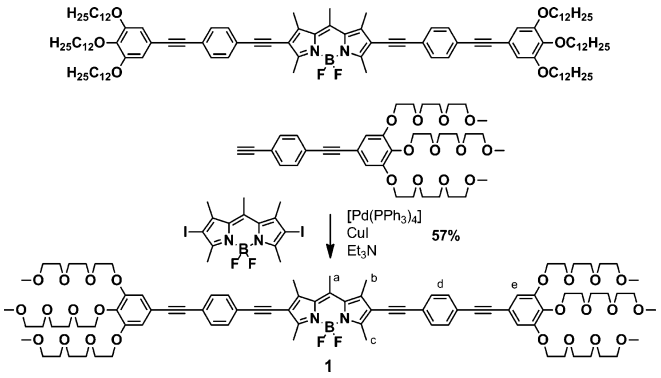

Scheme 1. Synthesis of the target BODIPY-OPE amphiphile **1**.

(Scheme 1, top). Our π-conjugated system self-assembles in nonpolar media such as cyclohexane into needle-like associates primarily driven by π–π interactions involving the BODIPY and OPE fragments.[9a] The high solubility of the nonpolar OPE-BODIPY in cyclohexane (≈30 mM) and, consequently, the absence of strong solvophobic interactions induces a moderate value of binding constant ($K_a \approx 1\times10^4$ M^{-1}) in this solvent. This phenomenon appears to be responsible for the formation of one-dimensional associates in which the OPE and BODIPY fragments are forming slipped stacks leading to a zigzag-like arrangement within the fibres. An obvious next step would be to scrutinize whether this intriguing organization is influenced in water, a unique medium in which strong hydrophobic interactions are the chief driving force to create self-assembled structures. As a result of that, the expected self-assembled structures would feature confined areas that provide an ideal environment for hydrophobic or aromatic guest molecules to be encapsulated and released under certain external conditions.

Herein, we describe the aqueous self-assembly of a new amphiphilic oligophenyleneethynylene (OPE)-BODIPY derivative (**1**) into flexible fibre-like H-aggregates and their reversible transformation into rigid fibres or spherical nanoparticles upon addition of tetracene and anthracene, respectively, which is accompanied by a change in the encapsulation mechanism from isodesmic to cooperative.

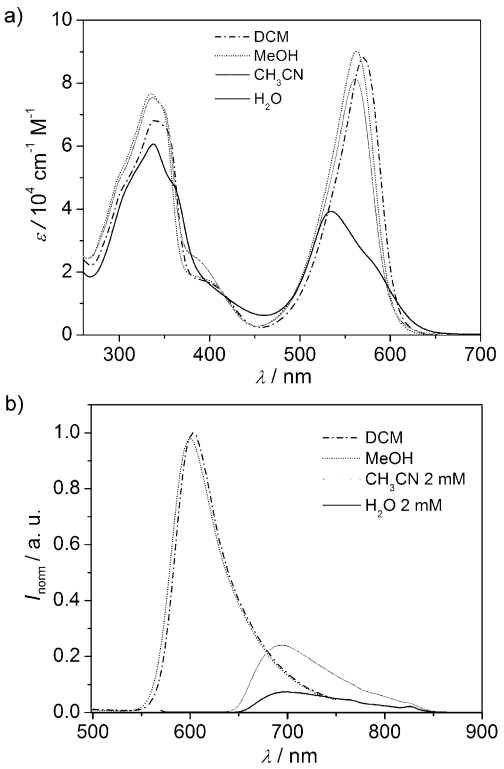

Figure 1. a) UV/Vis (1×10^{-5} M, 298 K) and b) emission spectra of **1** (1×10^{-5} M and 2 mM, 298 K) in different solvents. For (a), all concentrations are 1×10^{-5} M.

Results and Discussion

Amphiphile **1** (Scheme 1) has been synthesized by a Sonogashira cross-coupling reaction[18] of 2,6-diiodo-BODIPY (**2**)[19] and triethyleneglycol (TEG)-substituted OPE derivative **3**[20] (see Supporting Information) in 57% yield and fully characterized by ^{1}H and ^{13}C NMR, MALDI-TOF, high resolution ESI, UV/Vis and fluorescence spectroscopy (see Supporting Information).

The optical properties of **1** have been analysed by UV/Vis and fluorescence spectroscopy in different solvents. The UV/Vis spectra show the characteristic absorption bands of both OPE (≈330–340 nm) and BODIPY fragments (≈570 nm ($S_0\rightarrow S_1$ transition) and ≈410 nm ($S_0\rightarrow S_2$ transition); Figure 1 a and Table 1). No significant spectral changes are observed upon solvent variation with the exception of polar acetonitrile and water (Figure 1 a, Table 1 and Figure S1 in the Supporting Information). For both solvents, the $S_0\rightarrow S_1$ transition corresponding to the BODIPY core is broadened and blue-shifted. This trend is much more pronounced in water, in which a red-shifted shoulder at about 600 nm is also noticeable (Figure 1 a). The hypsochromic shift of the absorption maximum in water along with the appearance of a shoulder at 590 nm indicates a side-on arrangement of the molecules into H-aggregates with partial allowance of the lower energy transition due to a twisted dye conformation within the stack.[21] Simultaneously, the transition at approxi-

Table 1. Optical properties of **1** in different solvents (1×10^{-5} M, 298 K).

Solvent	$E_T^{N\ 24}$	λ_{abs} [nm] OPE	λ_{abs} [nm] $S_0\rightarrow S_1$	ε [M^{-1} cm^{-1}]	λ_{em} [nm][a]	Stokes shift[b] [nm]	Φ_F[c]
$CHCl_3$	0.259	340	573	65730, 85800	612	39	0.74
CH_2Cl_2	0.309	340	570	68458, 88300	603	33	0.72
1,4-Dioxane	0.164	340	568	71053, 92500	610	42	0.71
THF	0.207	339	567	72051, 89100	604	37	0.70
MeOH	0.775	336	563	76669, 90000	600	37	0.62
CH_3CN	0.460	331	555	65592, 70658	598	43	0.48
H_2O	1.000	338	534	60610, 39200	647	113	0.01

[a] $\lambda_{ex}=\lambda_{abs}$. [b] $\lambda_{abs}(S_0\rightarrow S_1)-\lambda_{em}$. [c] $A<0.05$;[25] estimated error: ±2%.

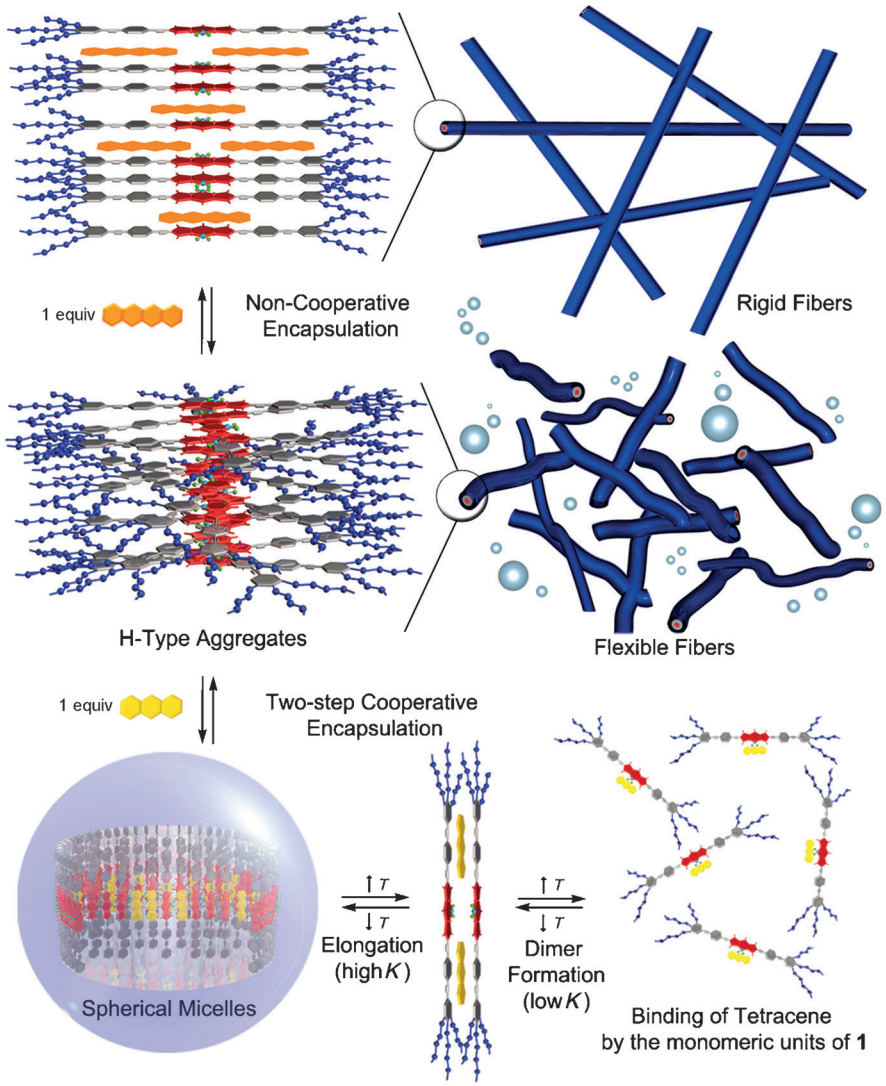

Scheme 2. Cartoon representation of the self-assembly of **1** into H-type aggregates and its reversible guest-dependent encapsulation processes.

mately 330–340 nm becomes sharper in water and acetonitrile, which is indicative of the planarization of the alkyne-aryl groups of the OPE fragments and represents a measure of the propensity of the π-system to self-assemble.[22] With regards to the emission properties, the spectra of **1** in acetonitrile and water are red-shifted and remarkably quenched compared to those in chloroform, dichloromethane or methanol (Figure 1b and Table 1). These findings suggest the formation of π-stacks with H-type excitonic coupling[23] between the BODIPY fragments (Scheme 2).

The self-assembly of **1** in solution was initially investigated through 1D and 2D NMR spectroscopy. The ^{1}H NMR spectrum of **1** in D_2O shows broad signals even at high temperature (353 K) and dilution (0.5 mM) as a result of a high degree of aggregation of **1** in aqueous medium. In contrast, the ^{1}H NMR signals in [D_3]acetonitrile are well-resolved and sensitive to concentration changes (Figure S2 in the Supporting Information). Figure 2a shows the concentration-dependent ^{1}H NMR experiments (400 MHz, 298 K) of **1** between 0.08 and 10 mM in CD_3CN. The broadening of most of the resonances is concomitant with the upfield shift of the aromatic signals upon increasing concentration (Figure 2a). The fact that the signals corresponding to the BODIPY core undergo the largest upfield shifts whereas the polar triethyleneglycol (TEG) chains are barely sensitive to concentration suggests the formation of H-type π-stacks with a slight rotation angle between the BODIPY units (see models in Figure 3 and Figure S3 in the Supporting Information). This hypothesis is supported by the presence of coupling signals between the aromatic protons (H_d) of the phenylene rings belonging to the OPE fragments and the methyl groups (H_b and H_c) of the BODIPY as well as between aromatic protons H_d and H_e in the rotating-frame Overhauser effect spectroscopy (ROESY) experiments of **1** in CD_3CN (Figure 2b and c, and Figures S4 and S5 in the Supporting Information). Such arrangement is considerably more favourable than the formation of slipped stacks, as strong solvophobic and π–π forces will be maximized if the dyes are arranged in a parallel fashion. Transmission

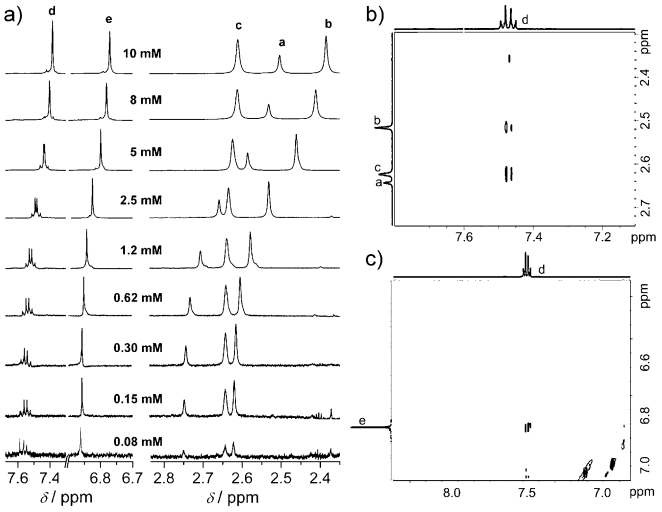

Figure 2. a) Partial ^{1}H NMR spectra of **1** at different concentrations (CD_3CN, 400 MHz, 298 K). Details of ROESY NMR spectrum of **1** (CD_3CN, 600 MHz, 4 mM, 298 K) showing the coupling signals of methyl groups H_b and H_c with aromatic protons H_d (b) and between aromatic protons H_d and H_e (c).

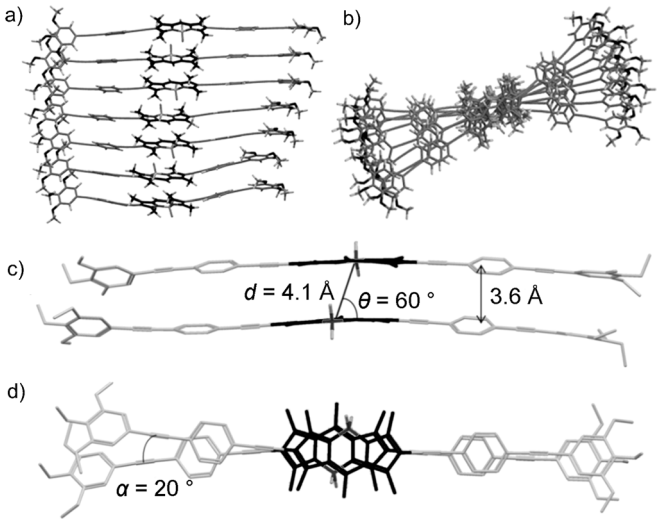

Figure 3. Force field optimized-geometry of seven molecules of amphiphilic OPE-BODIPY derivative **1**, a) side and b) top views and for two molecules c) side and d) top views (Macromodel).

electron microscopy (TEM) studies on a carbon-coated copper grid show the appearance of a network composed of elongated supramolecular objects with lengths up to about 300 nm, which is in agreement with NMR experiments (Figure S6 in the Supporting Information).

The self-assembly of **1** in water has been analysed in detail by temperature-dependent UV/Vis experiments, as this method covers the concentration range in which the transition from monomeric to H-aggregated species of **1** takes place. The spectral changes have been monitored by cooling down aqueous solutions of **1** at four different concentrations (1–4× 10^{-5} M) at a rate of 0.5 K min^{-1}. Above 343 K, the TEG chains are dehydrated as a consequence of the lower critical solution temperature (LCST) in water and less soluble species are formed.[26] However, the monomer-to-aggregate transition of **1** in water can be fully tracked if the solutions are slowly cooled down from 338 to 275 K (Figure 4a and Figures S7 and S8 in the Supporting Information). With decreasing temperatures, the sharpening of the OPE transition at 338 nm is accompanied by the hypsochromic shift of the $S_0 \rightarrow S_1$ transition corresponding to the BODIPY unit from 549 to 539 nm (Figure 4a). Additionally, the shoulder at 590 nm is absent at high temperature and becomes progressively more pronounced as the temperature decreases, indicating the excitonic coupling of the BODIPY units in a twisted H-type fashion. The appearance of isosbestic points at approximately 300 and 550 nm is indicative of equilibrium between monomeric and aggregated species. The thermodynamic parameters associated to the self-assembly process of **1** in water (see Table 2) have been determined by fitting the molar absorptivity (ε) against temperature at 520 nm to the isodesmic model.[27] According to this model, all binding events are isoenergetic. At room temperature, binding constants (K_a) ranging from of 0.9 to 1.5×10^6 M^{-1} and a melting temperature (T_m) of about 314–317 K have been calculated (Table 2).

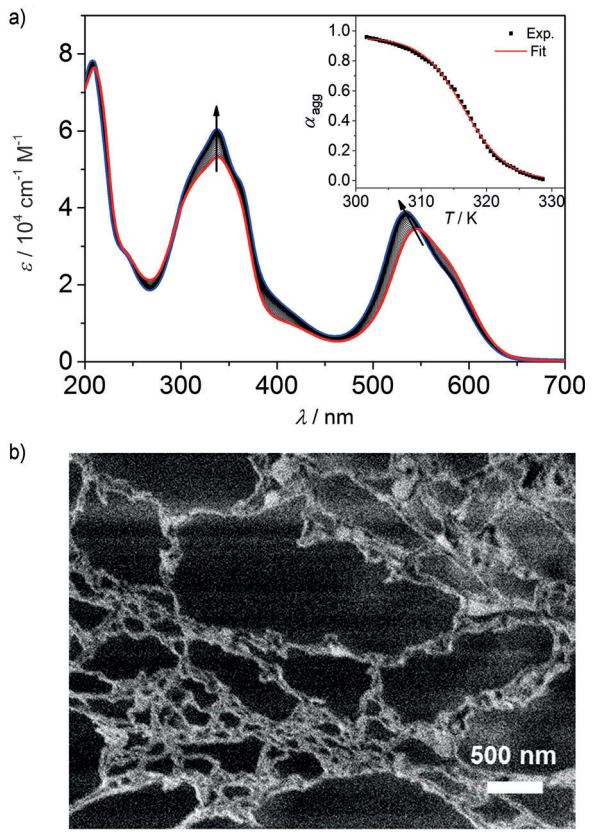

Figure 4. a) Temperature-dependent UV/Vis studies of **1** in water (3×10^{-5} M). Arrows indicate spectral changes upon temperature decrease. Inset: Fitting of the fraction of aggregated species (α_{agg}) against T at 520 nm to the isodesmic model. b) Cryo-SEM image of **1** prepared from water solution (5×10^{-5} M, 123 K).

Table 2. Thermodynamic parameters K_a, T_m, ΔH°, ΔG° and ΔS° obtained from the temperature-dependent UV/Vis experiments of BODIPY in water at different concentrations (298 K, λ = 520 nm).

Conc. [M]	K_a [M^{-1}]	T_m [K]	DP_N	ΔH [kJ mol^{-1}]	ΔS [J mol^{-1} K^{-1}]	ΔG [kJ mol^{-1}]
1×10^{-5}	1.0×10^6	314.4	1.41	−155.2	−405.8	−34.25
2×10^{-5}	1.3×10^6	314.9	1.42	−192.8	−530.1	−34.80
3×10^{-5}	0.9×10^6	315.4	1.42	−197.5	−548.6	−34.02
4×10^{-5}	1.5×10^6	316.7	1.42	−182.0	−492.6	−35.17

The aggregate size in solution has been determined by dynamic light scattering (DLS). In accordance with previous NMR and UV/Vis experiments, DLS studies demonstrate that **1** forms self-assembled structures in both acetonitrile and water at a concentration of 2 mM, with the average particle sizes being considerably larger in the latter (≈250 nm for acetonitrile and ≈1100 nm for water) as a result of increased hydrophobic interactions (Figure 5 and Figure S9 in the Supporting Information). For both solvents, the fact that the size distribution is dependent on the scattering angle strongly suggests the formation of anisotropic one-dimensional aggregates.[15a,28]

The morphology of the aggregates formed by **1** at a concentration of 5×10^{-5} M in water has been examined by cryogenic

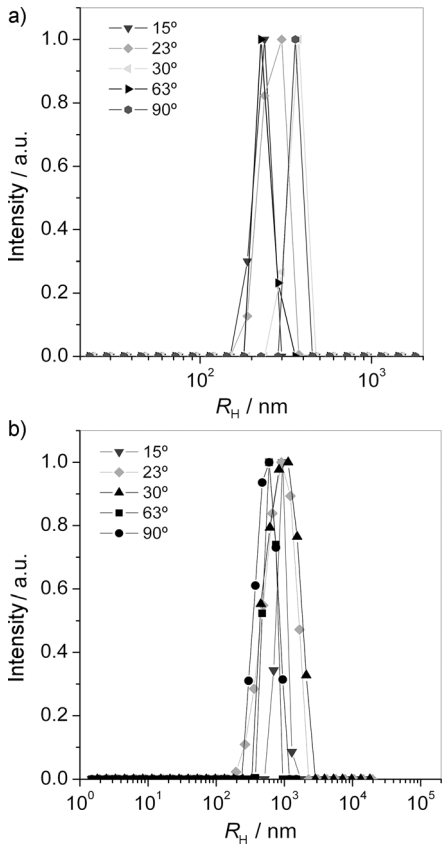

Figure 5. Size distribution from CONTIN analysis of the autocorrelation function of **1** a) in acetonitrile and b) in water (2 mM, 298 K) from DLS experiments.

scanning electron microscopy (Cryo-SEM) at 123 K. The images show the appearance of flexible fibrillar associates with diameters ranging from approximately 7 to 40 nm and lengths of several microns (Figure 4b and Figure S10 in the Supporting Information). The thinnest aggregates (6–7 nm) possess a single-molecule width and grow into thicker bundles of fibres facilitated by lateral interactions between the peripheral TEG chains. No significant changes in the morphology of the associates or gelation are observed up to approximately 1–2 mM, whereas above this point the aggregates formed precipitate out of solution.

To shed some light on the arrangement of the monomeric units of **1** within the fibrillar associates, we performed force field calculations (Macro Model, Amber). The energy-optimized structure of a set of seven monomeric units shows the formation of extended H-type aggregates in which the BODIPY units are stacked on top of each other with a small rotation angle (Figure 3 and Figure S3 in the Supporting Information). In this arrangement, the F–B–F fragments of the BODIPY chromophores are consecutively oriented to opposite sides to prevent steric repulsions, in accordance with previous studies.[8] The centre-to-centre distance between two adjacent molecules in the stack is 3.5 Å, and the slip angles that result from the rotational (α) and translational (θ) offset of two parallel-arranged molecules are 20° and 60°, respectively (Figure 3c and d and Figure S3 in the Supporting Information). This organization is in good agreement with the optical signatures of the H-aggregates with a twisted arrangement of the chromophores within the stack.

The hydrophobic interior of the fibrillar assemblies formed by amphiphile **1** in water can be ultimately exploited to encapsulate aromatic guest molecules. As hydrophobic guest, we initially chose a polycyclic aromatic hydrocarbon (tetracene) due to its appropriate small size and absorption in the UV/Vis region, which is complementary to the spectral features of amphiphile **1**. When one or two equivalents of tetracene are added to an aggregate solution of **1** at a concentration of 3×10^{-5} M in water, an immediate solubilisation of the hydrophobic dye is observed, indicating that an effective uptake of the guest molecules by the fibrillar assemblies takes place. The equimolar solution remains clear for several weeks without any sign of precipitation, suggesting the formation of stable co-assemblies. However, the addition of a higher amount of tetracene (above 1.5–2 equivalents) results in the formation of precipitates, clearly indicating that the excess molecules of tetracene can no longer be entrapped by the fibrillar assemblies of **1**. The encapsulation process has been monitored by UV/Vis experiments. After addition of one equivalent of tetracene to the aqueous solution of **1**, only slight spectral changes are observed (Figure 6a).

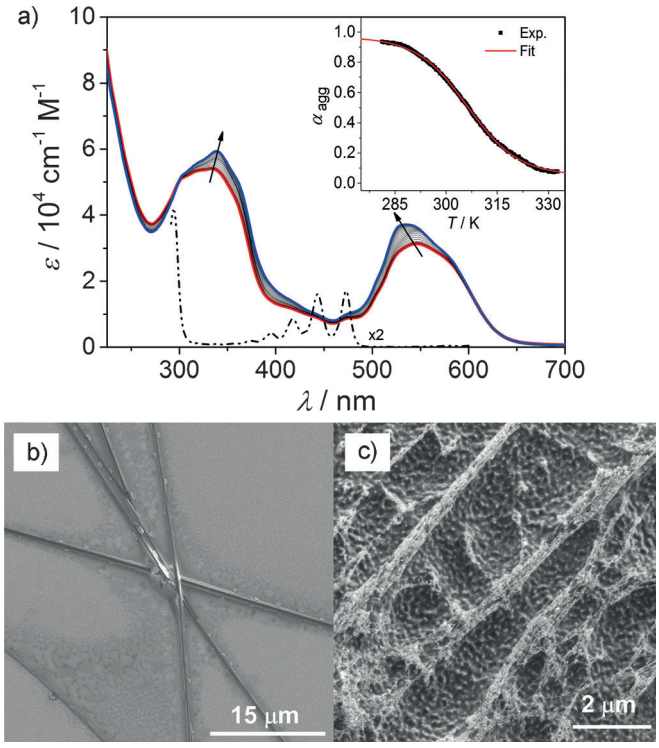

Figure 6. a) Temperature-dependent UV/Vis studies of **1** in aqueous solution (3×10^{-5} M) containing one equivalent of tetracene. Arrows indicate spectral changes upon temperature decrease. Dash-dotted line: UV/Vis spectra of tetracene in THF. Inset: Fitting of the spectral changes at 510 nm to the isodesmic model. b) SEM and c) cryo-SEM images of **1** mixed with one equivalent of tetracene (water, 1×10^{-5} M).

Upon closer inspection, we noticed the appearance of new maxima of relatively low intensity at approximately 480, 510 and 530 nm that are to some extent hidden below the $S_0 \rightarrow S_1$ transition of the BODIPY fragments of **1** (Figure 6a). These new maxima correspond to the absorption of the tetracene units (Figure 6a and Figures S11 and S12 in the Supporting Information) and are remarkably red-shifted ($\approx$20–50 nm) compared to those of the parent guest molecules in tetrahydrofuran (dash-dotted spectrum in Figure 6a), which accounts for a strong interaction between the molecules of **1** and tetracene. This has been demonstrated by analysing the aggregation behaviour of tetracene in isolation in THF/water mixtures at 1×10^{-5} M. The original absorption spectrum of tetracene in THF remains unchanged up to a maximum amount of 70% water (Figure S13 in the Supporting Information). Above this point, a significant drop in intensity and red-shift of the absorption spectra can be observed, which can be assigned to aggregate formation at high water content driven by hydrophobic interactions (Figure S13 in the Supporting Information). However, precipitation occurs only some minutes after water addition for all mixtures containing more than 20% of water, indicating that tetracene molecules are by themselves not stable in aqueous mixtures. Interestingly, the absorption maxima of tetracene in isolation in its aggregated state before precipitation closely match those observed in the mixtures with amphiphile **1** in pure water. To analyse this, we have subtracted the spectrum of **1** from the equimolar mixture of **1** and tetracene in water (inset of Figure S13 in the Supporting Information). The resulting maxima in the region between 400 and 550 nm approximately match those of tetracene in an aggregated form, thus demonstrating that tetracene exists in an aggregated state upon encapsulation.

We also observed a simultaneous drop in absorption of the BODIPY transition and a remarkable scattering in the region above 650 nm as a result of precipitation effects when more than 1 equivalent of tetracene was added to the aqueous solution of **1** (Figure S11 in the Supporting Information). This phenomenon strongly suggests a 1:1 binding stoichiometry between the aggregates of **1** and tetracene, which is also supported by titration experiments in water/THF (99.9:0.1) mixtures. To perform these studies, we have prepared a concentrated ($\approx$3 mM) solution of tetracene in THF and added it to a 300-fold more diluted solution of **1** in water, so the total amount of THF during the titration process is almost negligible (0.1%). Upon guest addition, the maxima at 330 and 550 nm decrease in intensity up to around 0.8–1.1 equivalents of guest, suggesting that the maximum amount of bound dye molecules is one equivalent. Unfortunately, Job plot analysis didn't result in a clear maximum and the exact stoichiometry cannot be determined by this method. However, the variation in absorption at 536 nm upon tetracene addition can be fitted to a 1:1 binding isotherm (Figure S14 in the Supporting Information) yielding a binding constant value of 8×10^5 M.

The reversibility of the encapsulation process has been analysed in detail by temperature-dependent UV/Vis experiments at concentrations between 2 and 5×10^{-5} M. On cooling down an equimolar mixture of **1** and tetracene in water from 338 to 278 K at 0.5 K min^{-1}, the maxima at 550 and 336 nm sharpen whereas the diagnostic bands of tetracene become more evident (Figure 6a and Figures S15 and S16 in the Supporting Information). The appearance of an isosbestic point at about 317 nm suggests equilibrium between well-defined species. The encapsulation mechanism has been followed by monitoring the spectral changes at a given wavelength (510 nm) with temperature. By following this procedure at four different concentrations (see above), cooling curves with a clear sigmoidal shape were obtained, which can be accurately fitted to a Boltzmann function (inset of Figure 6a and Figure S16 in the Supporting Information) and support the existence of a reversible isodesmic co-assembly process.[29] Application of this model to the temperature-dependent absorption changes affords binding constants (K_a) ranging from 4.7×10^4 M^{-1} to 1.7×10^5 M^{-1}. All thermodynamic parameters associated to this co-assembly process are shown in Table 3. With these overall data in hand, we

Table 3. Thermodynamic parameters associated to the self-assembly process of **1** and one equivalent of tetracene (water, 298 K, $\lambda = 510$ nm).

Conc. [M]	K_a [M^{-1}]	T_m [K]	DP_N	ΔH [kJ mol^{-1}]	ΔS [J mol^{-1}]	ΔG [kJ mol^{-1}]
2×10^{-5}	1.7×10^5	304.4	1.41	−115.7	−288.8	−29.8
3×10^{-5}	5.6×10^4	306.5	1.42	−94.4	−225.6	−27.1
4×10^{-5}	6.0×10^4	308.6	1.41	−102.1	−251.5	−27.7
5×10^{-5}	4.7 x10^4	309.2	1.42	−98.3	−240.2	−26.7

can extract two important conclusions: 1) The stability of the co-assemblies of **1** and tetracene is considerably lower than the fibres of **1** in isolation, as the latter binding constant is 10-fold higher than that associated to its mixture with tetracene. Most likely, the intercalation of tetracene units within the H-aggregates formed by **1** decreases the degree of packing of the molecules of **1** in the structure, thereby reducing the value of binding constant of the system. 2) The binding constant of the 1:1 complex formed by **1** and tetracene determined by titration experiments (8×10^5 M) is higher than that associated to the co-assembly (4.7×10^4–1.7×10^5 M) extracted from temperature-dependent UV/Vis studies. This implies that the monomeric units of **1** have a higher propensity to interact with the encapsulated tetracene guest molecules rather than with themselves within the co-assembled structures. Therefore, it is expected that a temperature increase would induce the disassembly of the co-assembled structures and the release of the 1:1 **1**/tetracene complexes as small fragments. This assumption is supported by the fact that even at high temperature (338 K) the water-insoluble tetracene molecules do not precipitate out of solution, indicating that they should be in some way shielded by the monomeric units of **1**.

The changes in the morphology of the fibrillar associates of **1** upon addition of tetracene have been investigated by SEM and cryo-SEM studies and are depicted in Figure 6b and c. The SEM images of an equimolar mixture of **1** and tetracene show that the initially flexible fibres of **1** dramatically stiffen upon addition of tetracene, whereas their length (several microns)

and width (40–500 nm) become larger than those of the pristine fibres of **1** (Figure 6b and Figure S17 in the Supporting Information), as a result of stronger hydrophobic interactions. The aromatic tetracene units are most likely randomly packed within the hydrophobic domain of the fibres, leading to an increased rigidity of the system, as shown in Scheme 2, top. Cryo-SEM images of this mixture reveals that the stiff associates of **1** and tetracene are in turn composed of thinner filaments that grow laterally into bundles through interactions between the TEG chains (Figure 6c and Figure S18 in the Supporting Information). DLS studies demonstrate that the average aggregate size of the mixed assembly (≈1300 nm) is comparable to that of **1** in isolation (≈1100 nm, Figure S19 in the Supporting Information), which is in full agreement with UV/Vis and SEM investigations.

We next questioned whether the encapsulation mechanism and morphology of the aggregates formed upon guest addition would be dependent on the size of the hydrophobic guest molecule. However, In the course of the encapsulation experiments of tetracene, we found out that the spectral features of tetracene overlap with those of the BODIPY fragments of **1**, making the process rather difficult to follow. To overcome this issue, we envisaged that a slightly shorter hydrophobic polycyclic aromatic hydrocarbon, anthracene, would be a better match to our BODIPY-OPE amphiphile **1**, both from a geometrical and electronic point of view. Similarly to tetracene, the addition of up to two equivalents of anthracene to an aqueous aggregate solution of **1** results in the solubilisation of the dye molecules by the aqueous aggregates of **1**, indicating an effective encapsulation of anthracene as well. Titration experiments in water containing traces of THF (0.1%) show the reduction of the BODIPY and OPE maxima upon addition of anthracene and the appearance of two isosbestic points at 300 and 506 nm (Figure S20 in the Supporting Information). Job plot analysis reveals a 1:1 stoichiometry between **1** and anthracene (Figures S21 and 22 in the Supporting Information). The spectral changes observed during the titration studies at 536 nm can be fitted to a 1:1 binding isotherm (Figure S20 in the Supporting Information) yielding a value of binding constant (8×10^5 M) that is very similar to that associated to tetracene binding.

To analyse in detail the mechanistic pathways taking place during the encapsulation process, we have investigated an equimolar mixture of **1** and anthracene through temperature-dependent UV/Vis experiments in water. At low temperature and similarly to tetracene, slight spectral changes are observed upon encapsulation, as most of the diagnostic maxima of anthracene (for comparison see the UV/Vis spectrum of anthracene in THF in Figure 7a) overlap with the absorption of the OPE fragments between 250 and 400 nm (see blue spectrum in Figure 7a). Nevertheless, a clear shoulder at approximately 400 nm that corresponds to the anthracene moiety can be distinguished, which supports the effective solubilisation of the guest. The absorption maxima of encapsulated anthracene, determined by subtracting the spectrum of **1** from the 1:1 **1**/anthracene mixture, is around 20 nm red-shifted compared to those in pure THF (inset of Figure S23 in the Supporting Information). Additionally, the absorption maxima of anthracene upon encapsulation closely match those of anthracene alone in an aggregated state in THF/water mixtures when the water content exceeds 90%, again demonstrating that anthracene exists in a self-assembled state in the mixture with **1** (Figure S23 in the Supporting Information). Nevertheless, due to the low solubility of anthracene in aqueous mixtures, precipitation occurs only some minutes after water addition.

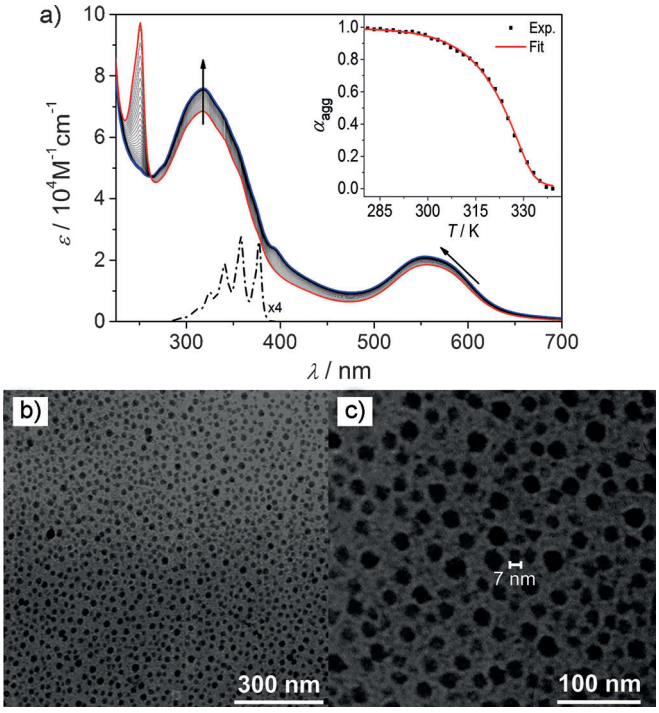

Figure 7. a) Temperature-dependent UV/Vis studies of **1** in aqueous solution (2×10^{-5} M) containing one equivalent of anthracene. Arrows indicate spectral changes upon temperature decrease. Dash-dotted line: UV/Vis spectra of anthracene in THF. Inset: Fitting of the spectral changes at 555 nm to the ten Eikelder–Markvoort–Meijer model. b) and c) TEM images of **1** and one equivalent of anthracene on carbon-coated copper grid (water, 1×10^{-5} M).

On the other hand, heating the 1:1 mixture of **1** and anthracene solution up to 338 K, leads to more significant changes in the absorption spectra compared to low temperature (see red spectrum in Figure 7a). For instance, the diagnostic transition of anthracene at 250 nm dramatically increases upon increasing temperature, which indicates that at high temperatures the anthracene units are released from the supramolecular aggregates of **1** (Figure 7a). The fact that the original spectrum (see blue line in Figure 7a) is recovered upon cooling down the solution back to 278 K along with the appearance of an isosbestic point at 268 nm indicates a reversible equilibrium between free and encapsulated guest species.

To our surprise, the co-assembly mechanism of anthracene proved to be significantly different when an equimolar mixture of **1** and anthracene was slowly cooled down from 338 to 278 K (rate = 0.5 K min^{-1}) at four different concentrations ($1–4\times10^{-5}$ M, Figures S24 and S25 in the Supporting Information). In sharp contrast to the behaviour of tetracene, the plot of fraction of aggregated molecules (α_{agg}) against temperature for all

concentrations at 555 nm is non-sigmoidal in shape, suggesting a cooperative co-assembly process (inset in Figure 7a and Figure S25). The cooling curve has been analysed by applying the nucleation–elongation model developed by ten Eikelder, Markvoort, Meijer and co-workers.[30] This mechanism assumes that after an initial thermodynamically unfavourable dimerization process (nucleation) described by an association constant K_2, a highly favourable cooperative growth (elongation) with a much larger binding constant (K) takes place. Application of this model to our experimental data allows us to calculate the thermodynamic parameters of the co-assembly process (Table 4), and demonstrates that the encapsulation of anthracene is cooperative. This intriguing guest-dependent change in the encapsulation mechanism anticipates that upon addition of anthracene new aggregates with a higher degree of organization should be formed, as cooperative effects often lead to supramolecular structures with a higher degree of internal order compared to non-cooperative counterparts.[13]

Table 4. Thermodynamic parameters K_2, K, σ, T_e, ΔH°, ΔH°_{nucl} and ΔS° obtained from temperature-dependent UV/Vis experiments of **1** and one equivalent of anthracene (water, $\lambda = 555$ nm) on the basis of the ten Eikelder–Markvoort–Meijer model.

Conc. [M]	ΔH°_{nucl} [kJ mol^{-1}]	ΔH° [kJ mol^{-1}]	ΔS° [J mol^{-1} K^{-1}]	T_e [K]	K_2 [M^{-1}]	K [M^{-1}]	σ
1×10^{-5}	−19.12	−82.77	−153	332.2	1400	3.1×10^{6}	4.5×10^{-4}
2×10^{-5}	−14.22	−79.89	−152	330.9	4000	1.2×10^{6}	3.2×10^{-3}
3×10^{-5}	−23.18	−80.28	−155	331.8	78	9.0×10^{5}	8.7×10^{-5}
4×10^{-5}	−35.00	−65.93	−114	333.0	0.3	4.1×10^{5}	7.3×10^{-7}

On the basis of these data, the nucleation constant is considerably (10^3–10^5-fold) smaller than the elongation constant, indicating a high degree of cooperativity in the co-assembly process. To better understand this complex behaviour, we have compared the values of binding constant of anthracene with **1** and the binding constant of the elongation step at a concentration of 4×10^{-5} M. At this concentration, the K_a associated to anthracene binding (8×10^5 M^{-1}) is slightly higher than that of the elongation of the co-assembled structure (4×10^5 M^{-1}). According to these results, heating of the 1:1 mixture of **1** and anthracene initially leads to the disassembly of the supramolecular co-assembled structures, which then release the molecules of **1** and anthracene as bound complexes. These species (possibly dimers based on UV/Vis analysis using the ten Eikelder model) formed by **1** and anthracene could be considered to be the monomeric units that finally form the supramolecular aggregate in a further elongation step (Scheme 2).

The influence of the co-assembly mechanism on the aggregate morphology has been investigated by SEM and TEM imaging. It is clear that the existence of cooperative effects in the co-assembly of anthracene should be reflected in aggregates with a distinctly new morphology. In fact, cryo-SEM images (Figure S26 in the Supporting Information) of **1** and one equivalent of anthracene reveal the formation of relatively monodisperse spherical nanoparticles with diameters between 7–15 nm, which are in agreement with the values observed by DLS (Figure S27 in the Supporting Information). These associates are most likely formed by strong π–π stacking between the OPE segments and the aromatic guest units, further stabilized by hydrogen bonding between the TEG chains and surrounding water molecules, as shown in Scheme 2. The smallest aggregates (6–7 nm) perfectly match the length of the OPE-BODIPY derivative **1** whereas the largest ones (15–20 nm) appear to arise as a result of the agglomeration of individual micelles into larger clusters. TEM images are in perfect agreement with cryo-SEM studies, and regular spherical associates with diameters between 6 and 20 nm can be observed (Figure 7b and c and Figure S28 in the Supporting Information).

Conclusion

In summary, we have described the self-assembly of a new amphiphilic oligophenyleneethynylene (OPE)-BODIPY derivative into fibrous aggregates in water. A wide range of experimental techniques (1D and 2D NMR spectroscopy, UV/Vis spectroscopy, fluorescence spectroscopy, DLS, Cryo-SEM and theoretical calculations) demonstrate the formation of extended H-type aggregates in water and acetonitrile driven by π–π and hydrophobic interactions. For the first time, the detailed thermodynamic analysis of an aqueous supramolecular polymer based on a BODIPY derivative has been reported. The interior of the resulting fibre-like associates provides an ideal hydrophobic environment for the entrapment of aromatic guest molecules driven by the hydrophobic effect. Upon encapsulation of tetracene, the flexibility of the fibres is reduced due to increased π–π and hydrophobic interactions between host and guest, resulting in a non-cooperative co-assembly process as demonstrated by detailed analysis of the UV/Vis spectral changes and supported by DLS and SEM studies. Surprisingly, the encapsulation of a slightly smaller aromatic guest (anthracene) under the same conditions turned out to be significantly different, as its co-assembly mechanism with **1** is a highly cooperative process. According to our analysis of titration and temperature-dependent UV/Vis studies, this process can be divided in three steps: at high temperatures the most favourable event is the binding of tetracene by the monomeric units of **1**, helping them to become soluble in water. These 1:1 complexes then dimerize when the temperature is decreased (nucleation) and ultimately elongate in a much more favourable step into spherical nanoparticles of 7–15 nm size in which the anthracene units are encapsulated in the interior, as demonstrated by microscopy studies (SEM, TEM) and DLS. This change in the co-assembly mechanism may be attributed to the fact that the molecules of **1** can no longer be fixed in a preferred direction as a result of decreased π–π interactions by addition of a smaller guest, leading to more stable, discrete assemblies. Our results bring to light that subtle changes in the molecular structure of the guest can lead to a significant modification of the co-assembly mechanism and, in turn, the resulting morphology of the co-aggregates. The application of some of these concepts to control the encapsulation and release of guest molecules might be rel-

evant to design biocompatible drug delivery systems in the near future.

Experimental Section

General methods

All solvents were dried according to standard procedures. Reagents were used as purchased. All air-sensitive reactions were carried out under argon atmosphere. Flash chromatography was performed using silica gel (Merck Silica 60, particle size 0.04–0.063 nm). Analytical thin layer chromatography (TLC) was performed on ALUGRAM Xtra SIL G/UV254 sheets supplied by Macherey–Nagel. NMR spectra were recorded on a Bruker Avance 400 (1H: 400 MHz; 13C: 100.6 MHz) or Bruker DMX 600 MHz spectrometer using partially deuterated solvents as internal standards. Coupling constants (J) are denoted in Hz and chemical shifts (δ) in ppm. Multiplicities are denoted as follows: s = singlet, d = doublet, t = triplet, m = multiplet. MALDI-TOF mass spectrometry was performed on an autoflex II instrument (Bruker Daltronik GmbH) in positive mode with a DCTB matrix. A microTOF focus instrument (Bruker Daltronik GmbH) was used to perform high resolution ESI-TOF mass spectrometry positive mode with chloroform/acetonitrile 1:1 for 4-(3,4,5-tris(triethyleneglycolmethylether)phenylethynyl)phenylethynyl)triisopropylsilane and 5-(4-ethynylphenylethynyl)-1,2,3-tris(triethyleneglycolmethylether)benzene and acetonitrile for compound **1** as solvents.

UV/Vis and fluorescence spectroscopy

For all spectroscopic measurements, spectroscopic grade solvents (Uvasol) from Merck were used. The standard UV/Vis measurements were carried out on a PerkinElmer Lambda 35 at room temperature. λ is denoted in nm and ε in $M^{-1}cm^{-1}$. The steady-state fluorescence spectra were recorded on a PTI QM4–2003 fluorescence spectrometer and corrected against photomultiplier (type R928) and lamp intensity of the 75 W Xenon lamp (type Ushio UXL-75 XE). The fluorescence quantum yield was determined as the average value for three different excitation wavelengths using N,N′-di(2,6-diisopropylphenyl)-1,6,7,12-tetraphenoxyperylene-3,4:9,10-tetracarboxylic acid bisimide as reference (Φ_F) = 0.96 in $CHCl_3$) by applying high dilution conditions ($A < 0.05$).

DLS

DLS measurements were performed at room temperature on a Beckman Coulter N5 submicron particle analyzer equipped with a 25 mW Helium-Neon Laser (632.8 nm) using 10 mm Hellma quartz cuvettes and spectroscopic grade solvents.

SEM

SEM imaging was performed on a Carl Zeiss Microscope Ultra plus field emission scanning electron microscope (FESEM) equipped with a GEMINI® e-Beam column (Carl Zeiss NTS GmbH) operating at an accelerating voltage of 1–3 kV with an aperture size set from 30 kV to 7 or 10 μm to avoid excessive charging and radiation damage of the samples imaged. The sample was prepared by placing a drop of the solution of **1** and one equivalent of tetracene in water onto a silicon wafer, removing the solvent with filter paper and placing a drop of silver ink onto the sample.

Cryo-HRSEM

The sample **1** in water was applied to copper sample stage mounted to stub shuttle device. Prior to examination, the specimen was plunged into slush (mixture of solid/liquid nitrogen) and rapidly frozen. The sample was transferred in a sealed vacuum transfer device to the precooled stage of the preparation chamber (Quorum PP2000T) which is mounted on to the SEM. Controlled freeze-drying of the fractured surface was performed for 2 min at a temperature of −95 °C and at a pressure of $p \approx 10$–6 mbar. The specimen was cooled to −150 °C again and transferred into a SEM sample chamber maintained at about −150 °C. Images of the sample were taken using a Zeiss Ultra plus field emission scanning electron microscope operated at 1 kV with an aperture size set to 10 μm to avoid excessive charging and radiation damage of the areas imaged.

TEM

TEM measurements were performed on a Siemens Elmiskop 101 Electron Microscope, operating at an acceleration voltage of 80–100 kV. For the observation of aggregates, a drop of sample solution was placed on 400-mesh formvar copper grids coated with carbon. Negative staining was performed by addition of a drop of uranyl acetate aqueous solution (0.5 %) onto the copper grid.

Synthetic details and characterization

1-Bromo-4-(trimethylsilylethynyl)benzene, (4-(trimethylsilylethynyl)-phenylethynyl)triisopropylsilane, ((4-ethynylphenyl)ethynyl)triisopropylsilane, 5-bromo-1,2,3-tris(2-(2-(2-methoxyethoxy)ethoxy)ethoxy)benzene, 4-(3,4,5-tris(triethyleneglycolmethylether)phenylethynyl)phenylethynyl)triisopropylsilane, 5-(4-ethynylphenylethynyl)-1,2,3-tris(triethyleneglycolmethylether)benzene, 4,4-difluoro-1,3,5,7,8-pentamethyl-4-bora-3a,4a-diaza-s-indacene and 4,4-difluoro-2,6-diiodo-1,3,5,7,8-pentamethyl-4-bora-3a,4a-diaza-s-indacene were prepared following reported synthetic procedures and showed identical spectroscopic properties to those reported therein.[19,20]

Amphiphilic OPE-BODIPY (1): 62.6 mg (121.8 μmol, 1 equiv) 4,4-difluoro-2,6-diiodo-1,3,5,7-tetramethyl-4-bora-3a,4a-diaza-s-indacene, 176.4 mg (256 μmol, 2.1 equiv) 5-(4-ethynylphenylethynyl)-1,2,3-tris(triethyleneglycolmethylether)benzene, 7.04 mg (6.10 μmol, 0.05 equiv) tetrakis-(triphenylphosphine)palladium(0), 2.32 mg (12.18 μmol, 0.03 equiv) copper(I) iodide and 100.12 μL (732 μmol, 74.0 mg, 6 equiv) triethylamine were combined in 10 mL millipore water. The suspension was degassed and flushed with argon five times. Then, the reaction mixture was heated to 70 °C and stirred while the colour changed from red to deep purple. After three hours, the complete consumption of the starting material was monitored by TLC. Afterwards, the reaction mixture was extracted with 150 mL dichloromethane and the organic layer dried over $MgSO_4$. The solvent was removed under reduced pressure and the crude product purified by column chromatography (silica gel, $CHCl_3$/MeOH 98:2, $R_f = 0.16$). The purified product was dried by lyophilization of a water/dioxane solution giving a deep purple solid (114 mg, 68.6 μmol, yield: 57 %). ^{1}H NMR (400 MHz, CD_3CN, 298 K): $\delta = 7.52$ (m, 8H, H_d), 6.85 (s, 4H, H_e), 4.15 (m, 12H, H_f), 3.82 (m, 8H, H_g), 3.74 (m, 4H, $H_{g'}$), 3.70–3.47 (m, 48H, H_{h-k}), 3.32 (s, 6H, H_l), 3.31 (s, 12H, H_l), 2.70 (s, 3H, H_a), 2.66 (s, 6H, H_c), 2.57 ppm (s, 6H, H_b); ^{13}C NMR (100.6 MHz, CD_3CN, 298 K): $\delta = 157.0$, 153.6, 145.3, 143.7, 140.1, 132.9, 132.3, 132.1, 129.1, 124.0, 123.6, 116.3, 111.5, 97.0, 92.2, 88.8, 84.5, 73.3, 72.6, 71.4, 71.3, 71.2, 71.1, 71.0, 70.3, 69.7, 58.9, 17.7, 16.3, 13.8 ppm (t, $^4J(C,F) = 2.56$ Hz); MALDI-TOF: $m/z =$

1634.83; HRMS (ESI)$^+$ (acetonitrile): *m/z* calcd for $[C_{88}H_{121}BF_2N_3O_{24}]^+$: 1651.8432; found: 1651.8448 $[M+NH_4]^+$; UV/Vis (CH_2Cl_2): λ_{max} (ε) = 570 (88300), 340 (68500); fluorescence quantum yield (Φ_F) in CH_2Cl_2 = 0.67.

Acknowledgements

We are thankful to Prof. Frank Würthner for many helpful discussions, Ana Reviejo for graphic design and the Humboldt Foundation for financial support (Sofja Kovalevskaja Award).

Keywords: amphiphiles · aqueous self-assembly · encapsulation · supramolecular polymerization · π-conjugated systems

[1] a) A. B. Nepomnyashchii, A. J. Bard, *Acc. Chem. Res.* **2012**, *45*, 1844 – 1853; b) G. Ulrich, R. Ziessel, A. Harriman, *Angew. Chem.* **2008**, *120*, 1202 – 1219; *Angew. Chem. Int. Ed.* **2008**, *47*, 1184 – 1201; c) A. Loudet, K. Burgess, *Chem. Rev.* **2007**, *107*, 4891 – 4932.

[2] N. Boens, V. Leen, W. Dehaen, *Chem. Soc. Rev.* **2012**, *41*, 1130 – 1172.

[3] For recent examples see: a) K. K. Jagtap, N. Shivran, S. Mula, D. B. Naik, S. K. Sarkar, T. Mukherjee, D. K. Maity, A. K. Ray, *Chem. Eur. J.* **2013**, *19*, 702 – 708; b) Y. Xiao, D. Zhang, X. Qian, A. Costela, I. Garcia-Moreno, V. Martin, M. E. Perez-Ojeda, J. Bañuelos, L. Gartzia, I. Lopez Arbeloa, *Chem. Commun.* **2011**, *47*, 11513 – 11515.

[4] a) S.-L. Niu, C. Massif, G. Ulrich, P.-Y. Renard, A. Romieu, R. Ziessel, *Chem. Eur. J.* **2012**, *18*, 7229 – 7242; b) S.-L. Niu, C. Massif, G. Ulrich, R. Ziessel, P.-Y. Renard, A. Romieu, *Org. Biomol. Chem.* **2011**, *9*, 66 – 69.

[5] a) A. Kamkaew, S. H. Lim, H. B. Lee, L. V. Kiew, L. Y. Chung, K. Burgess, *Chem. Soc. Rev.* **2013**, *42*, 77 – 88; b) N. Adarsh, R. R. Avirah, D. Ramaiah, *Org. Lett.* **2010**, *12*, 5720 – 5723.

[6] a) T. Bura, N. Leclerc, S. Fall, P. Lévêque, T. Heiser, P. Retailleau, S. Rihn, A. Mirloup, R. Ziessel, *J. Am. Chem. Soc.* **2012**, *134*, 17404 – 17407; b) Y. Hayashi, N. Obata, M. Tamaru, S. Yamaguchi, Y. Matsuo, A. Saeki, S. Seki, Y. Kureishi, S. Saito, S. Yamaguchi, H. Shinokubo, *Org. Lett.* **2012**, *14*, 866 – 869; c) S. Kolemen, O. A. Bozdemir, Y. Cakmak, G. Barin, S. Erten-Ela, M. Marszalek, J.-H. Yum, S. M. Zakeeruddin, M. K. Nazeeruddin, M. Grätzel, E. U. Akkaya, *Chem. Sci.* **2011**, *2*, 949 – 954; d) S. Kolemen, Y. Cakmak, S. Erten-Ela, Y. Altay, Y. Brendel, M. Thelakkat, E. U. Akkaya, *Org. Lett.* **2010**, *12*, 3812 – 3815.

[7] a) B. Rybtchinski, *ACS Nano* **2011**, *5*, 6791 – 6818; b) A. P. H. J. Schenning, E. W. Meijer, *Chem. Commun.* **2005**, 3245 – 3258.

[8] a) I. Mikhalyov, N. Gretskaya, F. Bergstrçm, L. B.-Å. Johansson, *Phys. Chem. Chem. Phys.* **2002**, *4*, 5663 – 5670; b) D. Tleugabulova, Z. Zhang, J. D. Brennan, *J. Phys. Chem. B* **2002**, *106*, 13133 – 13138.

[9] a) A. Florian, M. J. Mayoral, V. Stepanenko, G. Fernández, *Chem. Eur. J.* **2012**, *18*, 14957 – 14961; b) H. Liu, J. Mack, Q. Guo, H. Lu, N. Kobayashi, Z. Shen, *Chem. Commun.* **2011**, *47*, 12092 – 12094; c) A. Nagai, K. Kokado, J. Miyake, Y. Chujo, *Macromolecules* **2009**, *42*, 5446 – 5452; d) A. Nagai, J. Miyake, K. Kokado, Y. Nagata, Y. Chujo, *J. Am. Chem. Soc.* **2008**, *130*, 15276 – 15278.

[10] a) L. Gai, H. Lu, B. Zou, G. Lai, Z. Shen, Z. Li, *RSC Adv.* **2012**, *2*, 8840 – 8846; b) J.-H. Olivier, J. Barberá, E. Bahaidarah, A. Harriman, R. Ziessel, *J. Am. Chem. Soc.* **2012**, *134*, 6100 – 6103; c) M. Benstead, G. A. Rosser, A. Beeby, G. H. Mehl, R. W. Boyle, *New J. Chem.* **2011**, *35*, 1410 – 1417; d) S. Frein, F. Camerel, R. Ziessel, J. Barberá, R. Deschenaux, *Chem. Mater.* **2009**, *21*, 3950 – 3959; e) F. Camerel, G. Ulrich, J. Barberá, R. Ziessel, *Chem. Eur. J.* **2007**, *13*, 2189 – 2200; f) F. Camerel, L. Bonardi, G. Ulrich, L. Charbonniere, B. Donnio, C. Bourgogne, D. Guillon, P. Retailleau, R. Ziessel, *Chem. Mater.* **2006**, *18*, 5009 – 5021; g) F. Camerel, L. Bonardi, M. Schmutz, R. Ziessel, *J. Am. Chem. Soc.* **2006**, *128*, 4548 – 4549.

[11] For examples of BODIPY-based nanoparticle assemblies in water, see: a) J.-H. Olivier, J. Widmaier, R. Ziessel, *Chem. Eur. J.* **2011**, *17*, 11709 – 11714; b) Y. Tokoro, A. Nagai, Y. Chujo, *Tetrahedron Lett.* **2010**, *51*, 3451 – 3454.

[12] a) K. Wunderlich, A. Larsen, J. Marakis, G. Fytas, M. Klapper, K. Müllen, *Small* **2014**, *10*, 1914 – 1919; b) A. Das, S. Ghosh, *Angew. Chem.* **2014**, *126*, 2068 – 2084; *Angew. Chem. Int. Ed.* **2014**, *53*, 2038 – 2054; c) B. Narayan, S. P. Senanayak, A. Jain, K. S. Narayan, S. J. George, *Adv. Funct. Mater.* **2013**, *23*, 3053 – 3060; d) L. Chen, K. S. Mali, S. R. Puniredd, M. Baumgarten, K. Parvez, W. Pisula, S. De Feyter, K. Muellen, *J. Am. Chem. Soc.* **2013**, *135*, 13531 – 13537; e) D. Görl, X. Zhang, F. Würthner, *Angew. Chem.* **2012**, *124*, 6434 – 6455; *Angew. Chem. Int. Ed.* **2012**, *51*, 6328 – 6348; f) J. B. Matson, S. I. Stupp, *Chem. Commun.* **2012**, *48*, 26 – 33; g) M. J. Mayoral, G. Fernandez, *Chem. Sci.* **2012**, *3*, 1395 – 1398; h) H.-J. Kim, T. Kim, M. Lee, *Acc. Chem. Res.* **2011**, *44*, 72 – 82; i) W. Zhang, W. Jin, T. Fukushima, A. Saeki, S. Seki, T. Aida, *Science* **2011**, *334*, 340 – 343; j) J.-H. Ryu, D.-J. Hong, M. Lee, *Chem. Commun.* **2008**, 1043 – 1054.

[13] T. Aida, E. W. Meijer, S. I. Stupp, *Science* **2012**, *335*, 813 – 817.

[14] a) S. S. Babu, V. K. Praveen, A. Ajayaghosh, *Chem. Rev.* **2014**, *114*, 1973 – 2129; b) J. A. Foster, J. W. Steed, *Angew. Chem.* **2010**, *122*, 6868 – 6874; *Angew. Chem. Int. Ed.* **2010**, *49*, 6718 – 6724; c) J. A. Foster, M. Piepenbrock Marc-Oliver, G. O. Lloyd, N. Clarke, A. K. Howard Judith, J. W. Steed, *Nat. Chem.* **2010**, *2*, 1037 – 1043; d) N. M. Sangeetha, U. Maitra, *Chem. Soc. Rev.* **2005**, *34*, 821 – 836.

[15] a) C. Rest, M. J. Mayoral, G. Fernandez, *Int. J. Mol. Sci.* **2013**, *14*, 1541 – 1565; b) M. R. Molla, S. Ghosh, *Chem. Eur. J.* **2012**, *18*, 9860 – 9869; c) T. Emiliano, P. Nandhini, G. D. Pantoş, K. M. S. Jeremy, *Faraday Discuss.* **2010**, *145*, 205 – 218; d) K. S. Moon, H. J. Kim, E. Lee, M. Lee, *Angew. Chem.* **2007**, *119*, 6931 – 6934; *Angew. Chem. Int. Ed.* **2007**, *46*, 6807 – 6810; e) J.-H. Ryu, H.-J. Kim, Z. Huang, E. Lee, M. Lee, *Angew. Chem.* **2006**, *118*, 5430 – 5433; *Angew. Chem. Int. Ed.* **2006**, *45*, 5304 – 5307.

[16] a) Y. Liu, B. Liu, J. Riesberg, W. Shen, *Macromol. Biosci.* **2011**, *11*, 1325 – 1330; b) C. DeForest, B. Polizzotti, K. Anseth, *Nat. Mater.* **2009**, *8*, 659 – 664; c) M. Cushing, K. Anseth, *Science* **2007**, *316*, 1133 – 1134.

[17] Z. Huang, H. Lee, E. Lee, S. K. Kang, J. M. Nam, M. Lee, *Nat. Commun.* **2011**, *2*, 459.

[18] *Metal-Catalyzed Cross-Coupling Reactions* (Eds.: F. Diederich, P. J. Stang), Wiley-VCH, Weinheim, **1998**.

[19] T. Yogo, Y. Urano, Y. Ishitsuka, F. Maniwa, T. Nagano, *J. Am. Chem. Soc.* **2005**, *127*, 12162 – 12163.

[20] C. Rest, M. J. Mayoral, K. Fucke, J. Schellheimer, V. Stepanenko, G. Fernández, *Angew. Chem.* **2014**, *126*, 716 – 722; *Angew. Chem. Int. Ed.* **2014**, *53*, 700 – 705.

[21] M. Kasha, H. R. Rawls, M. Ashraf El-Bayoumi, *Pure Appl. Chem.* **1965**, *11*, 371 – 392.

[22] a) Q. Chu, Y. Pang, *Macromolecules* **2005**, *38*, 517 – 520; b) A. Beeby, K. Findlay, P. J. Low, T. B. Marder, *J. Am. Chem. Soc.* **2002**, *124*, 8280 – 8284; c) M. Levitus, K. Schmieder, H. Ricks, K. D. Shimizu, U. H. F. Bunz, M. A. García-Garibay, *J. Am. Chem. Soc.* **2001**, *123*, 4259 – 4265.

[23] F. C. Spano, *Acc. Chem. Res.* **2010**, *43*, 429 – 439.

[24] C. Reichardt, *Chem. Rev.* **1994**, *94*, 2319 – 2358.

[25] K. Rurack, "Fluorescence Quantum Yields: Methods of Determination and Standards" in *Springer Series on Fluorescence Vol. 5* (Ed.: U. Resch-Genger), Springer-Verlag, Berlin Heidelberg, **2008**, pp. 101 – 145.

[26] a) A. Nagai, K. Kokado, J. Miyake, Y. Chujo, *J. Polym. Sci. Part A* **2010**, *48*, 627 – 634; b) T. Hirose, K. Matsuda, *Chem. Commun.* **2009**, 5832 – 5834.

[27] a) M. M. Smulders, M. M. L. Nieuwenhuizen, T. F. A. De Greef, P. van der Schoot, A. P. H. J. Schenning, E. W. Meijer, *Chem. Eur. J.* **2010**, *16*, 362 – 367; b) T. F. A. de Greef, M. M. J. Smulders, M. Wolffs, A. P. H. J. Schenning, R. P. Sijbesma, E. W. Meijer, *Chem. Rev.* **2009**, *109*, 5687 – 5754.

[28] G. Fernández, M. Stolte, V. Stepanenko, F. Würthner, *Chem. Eur. J.* **2013**, *19*, 206 – 217.

[29] F. García, L. Sánchez, *Chem. Eur. J.* **2010**, *16*, 3138 – 3146.

[30] a) H. M. M. ten Eikelder, A. J. Markvoort, T. F. A. de Greef, P. A. J. Hilbers, *J. Phys. Chem. B* **2012**, *116*, 5291 – 5301; b) A. J. Markvoort, H. M. M. ten Eikelder, P. A. J. Hilbers, T. F. A. de Greef, E. W. Meijer, *Nat. Commun.* **2011**, *2*, 509 – 517.

Received: February 7, 2014
Published online on July 14, 2014